JOURNAL OF MATERIALS SCIENCE: 30 (1995) 2227–2234

Study of lanthanum-deficient compositions in the systems La–Cu–O and La–Sr–Cu–O

S. A. ALCONCHEL, M. A. ULLA, E. A. LOMBARDO
Instituto de Investigaciones en Catálisis y Petroquímica, INCAPE (FIQ, UNL – CONICET), Santiago del Estero 2829, 3000 Santa Fe, Argentina

The effect of varying lanthanum composition upon the formation of the non-superconducting $La_{1.67}Sr_{0.33}Cu_2O_{5-\delta}$ and the stoichiometry variation tolerance of the ternary system $La_{2-x}Sr_xCuO_4$ (with $x=0$ and 0.15) were investigated using a variety of techniques. Results indicate that total conversion to La_2CuO_4 from freeze-dried precursors with an La:Cu = 2.00:1 ratio is achieved after sintering (1253 K, 12 h) and annealing in oxygen (773 K, 6 h). Small variations in the stoichiometry of solids $La_{2-x}Sr_xCuO_4$ with $x=0$ and 0.15 were detected. Lanthanum-deficient composition in the ternary system induces the formation of the non-superconducting phase whose stoichiometry is better represented by $La_{1.60}Sr_{0.40}Cu_2O_{5-\delta}$. The temperature-programmed reduction profiles of the cuprates can be associated with the formation of more or less stable intermediates.

1. Introduction

A solid with good superconducting properties should be a monophasic material with a well-defined stoichiometry. Deviations in the chemical composition usually lead to a phase segregation which is not completely overcome after sintering. On the other hand, the synthesis procedure may also lead to solids showing preferential deficiency in some of its components or the appearance of impurities. In many cases, these effects are so large as to impair the development of high-T_c superconducting phases. This is why the precise control of the stoichiometry is a key factor to obtain the best superconducting behaviour.

In a previous paper [1], we carried out a detailed study of the preparation of the freeze-dried precursors of the superconducting compound $La_{1.85}Sr_{0.15}CuO_4$ starting from the corresponding acetates. A most relevant observation was the fusion of strontium acetate and the complex decomposition mechanism of the copper salt leading to the appearance of a transient liquid phase at temperatures around 600 K. This leads to two undesirable side effects [2]: (i) the impossibility of decreasing the synthesis temperature of the superconducting oxide which was expected from the use of the cryochemical method, and (ii) the local composition fluctuations seem to generate lanthanum deficient regions where the non-superconducting ternary compound $La_{1.67}Sr_{0.33}Cu_2O_{5-\delta}$ develops.

Despite these difficulties it is possible to obtain monophasic oxides in the form of sintered pellets using powders calcined at 1253 K. The structural evolution observed in samples prepared under these synthesis conditions is consistent with the solid-state reaction between CuO, $La(OH)_3$ and $La_{1.67}Sr_{0.33}Cu_2O_{5-\delta}$ to yield total conversion to the superconducting oxide [2].

Further investigations [3] were performed to obtain single-phase powders by carefully designing and controlling the heating strategy used during the transformation of the precursor in the superconducting oxide.

The aim of the present work was to check the effect of varying lanthanum composition upon the formation of the non-superconducting compound $La_{1.67}Sr_{0.33}Cu_2O_{5-\delta}$ and the stoichiometry variation tolerance of the ternary system. Samples of $La_{2-x}Sr_xCuO_4$ ($x = 0$ and 0.15) were prepared starting from freeze-dried precursors with La:Cu ratios varying around the nominal atomic ratio. The non-superconducting phase $La_{1.67}Sr_{0.33}Cu_2O_{5-\delta}$ was also synthetized. The solids were characterized through X-ray diffraction (XRD), iodometric titration, scanning electron microscopy (SEM) and temperature-programmed reduction (TPR).

2. Experimental procedure

2.1. Sample preparation

Samples of $La_{2-x}Sr_xCuO_4$ (with $x = 0$ and 0.15) and $La_{1.67}Sr_{0.33}Cu_2O_{5-\delta}$ were prepared from high-purity (99.99%) acetates of lanthanum, strontium and copper by freeze-drying. Individual water solutions of each reactant were chemically analysed and mixed in different cation relations La:Cu as indicated in Table I. Binary and ternary solutions (total cation concentration 0.23 mol l^{-1}) were flash-frozen by atomization into a liquid-nitrogen vortex and dried under vacuum in a commercial freeze-dryer. More details have been given elsewhere [1].

The dried powders (precursors) were transferred to a transparent quartz tubular reactor (diameter 0.05 m and length 0.60 m) [2] and calcined at a final

0022–2461

TABLE I Stoichiometry ratios for La–Sr–Cu–O compounds prepared by the freeze-drying method

Sample	La	Sr	Cu
A	2.00	0.00	1
B	1.95	0.00	1
C	1.90	0.00	1
D	1.85	0.00	1
E	1.70	0.00	1
F	1.75	0.15	1
G	1.80	0.15	1
H	1.95	0.15	1
I	1.67	0.33	2

temperature of $T_f = 1253$ K for 8 h. The heating rate was 50 K min^{-1} upto 773 K and was then reduced to 5 K min^{-1} to T_f. The samples were slowly cooled to room temperature inside the oven at an estimated rate of 1 K min^{-1}. In all cases, the thermal treatment was conducted in flowing air up to 893 K and then in flowing oxygen to room temperature, with a flow rate of 400 ml (STP) min^{-1}.

The solids obtained were ground and pelletized (disc shape, diameter 12 mm, thickness 2–3 mm) at 490 MPa for 6 min. These pellets were sintered under oxygen (flow rate 400 ml (STP) min^{-1}) at $T_f = 1253$ K for 12 h. The heating rate was 5 K min^{-1}. The sintered samples were then slowly cooled inside the oven, always under an oxygen flow. Finally, the pellets were annealed in oxygen at 773 K for 6 h and again slowly cooled to room temperature, always in oxygen.

2.2. Sample characterization

The X-ray diffractograms (XRD) of the samples were obtained at room temperature with a Rich–Seifert (Model Iso-Debyeflex 2002) instrument, using CuK_α radiation ($\lambda = 0.1542$ nm) nickel filter and a scanning rate of 0.6° min^{-1}. To further check for the possible presence of trace impurities, selected regions of the diffractograms were scanned at a slower rate of 0.12° min^{-1} while saturating the signals of the main component.

The oxygen content of the calcined powders shown in Table I, was calculated using the procedure given by Appelman *et al.* [4]. Triplicate determinations of each sample were made.

The morphology of oxide A (Table I) before mechanical grinding was studied using a Jeol microscope (Model JSM-35C) operated at accelerating voltages of 20–25 kV. Small fragments of the sample were glued to a metallic sample holder using silver paint. The preparations were covered with a thin gold layer to improve observations.

TPR experiments were carried out on powders using a standard TPR apparatus [5] and a H_2/Ar (5/95 v/v%) stream (25 ml(STP) min^{-1}). For a typical measurement, 10 mg sample were loaded in a quartz reactor (diameter 7 mm) of the flow-through type. After connecting the reactor the whole TPR system, including tubing, gas manifold, and Gow-Mac (Model 13–002) thermal conductivity detector (TCD), was purged with the reducing gas for 2 h. The TCD output (hydrogen consumption) was recorded on a strip chart recorder.

3. Results

3.1. X-ray diffraction

The diffractogram (Fig. 1a) of sample A (La:Cu = 2.00:1) shows that the thermal decomposition of the amorphous freeze-dried precursor at 1253 K (8 h) leads to the formation of La_2CuO_4(PDF 38–709) [6]. Residual impurities such as $La(OH)_3$ (PDF 6-0585, 36-1481) and CuO (PDF 5-0661 and 41-254) were detected using slower scanning rates and sharply increasing the intensity scale (Fig. 1b).

Similar patterns were obtained for samples B–E with La:Cu < 2.00:1 (Table I). The impurity phases frequently observed were La $(OH)_3$, $La_2O_2CO_3$ (PDF 37-804) and occasionally CuO.

Sintering followed by oxygen annealing led to monophasic powders for La:Cu = 2.00:1 (Fig. 2a), 1.95:1 and 1.90:1 (Fig. 2.b) while lower ratios allowed the observation of the excess CuO (Fig. 2c).

In sample F (La:Sr:Cu = 1.75:0.15:1), together with the superconducting phase $La_{1.85}Sr_{0.15}CuO_4$ (PDF 39-1041), La_2O_3 (PDF 5-0602) and $La_{1.67}Sr_{0.33}Cu_2O_{5-\delta}$ (PDF 39–1498) appeared as impurities. The main diffraction lines appearing at $2\theta = 29.9°$ and 32.9°, respectively. After sintering and oxygen annealing, La_2O_3 disappeared but the non-superconducting compound was still there (Fig. 3a).

Increasing the lanthanum proportion (La:Sr:Cu = 1.80:0.15:1) leads essentially to the same impurities ($La(OH)_3$ replaces La_2O_3). In this case, however, sintering and oxygen annealing allowed the production of a monophasic oxide (Fig. 3b).

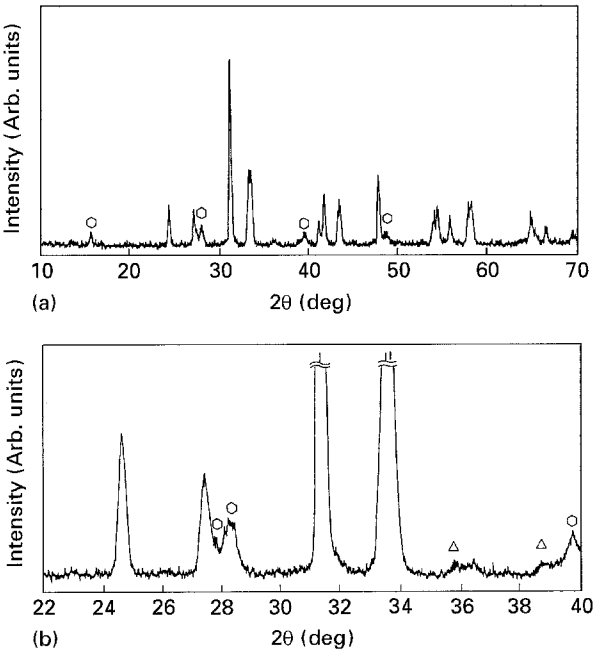

Figure 1 XRD patterns of sample A (La:Cu = 2.00:1) calcined at 1253 K for 8 h in oxygen. (a) $2\theta = 10°$–70° and (b) $2\theta = 22°$–40° (magnified intensity and slow scan). (○) $La(OH)_3$, (△) CuO.

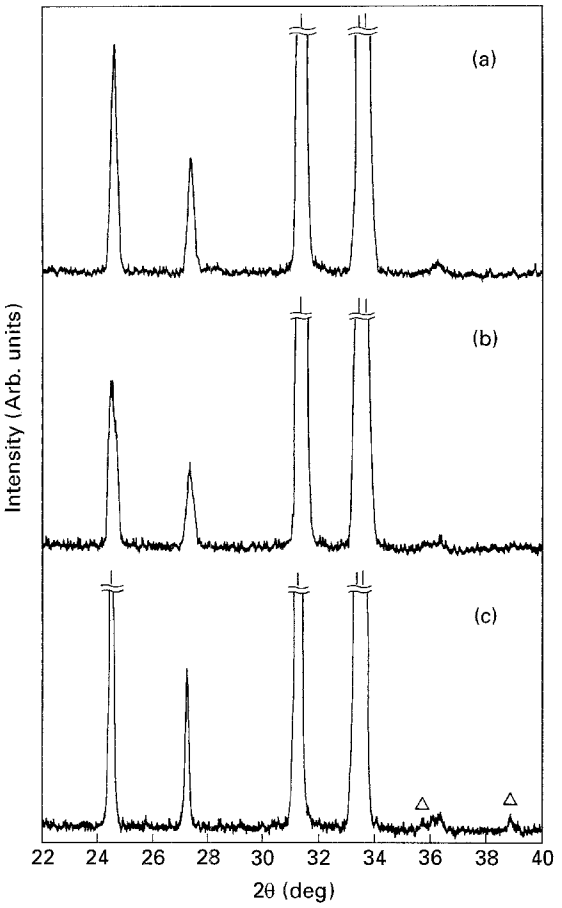

Figure 2 Magnified XRD patterns of binary oxides sintered at 1253 K for 12 h and annealed at 773 K for 6 h, both in oxygen. (a) Sample A (La:Cu = 2.00:1), (b) sample C (La:Cu = 1.90:1) and (c) sample D (La:Cu = 1.85:1). (△)CuO.

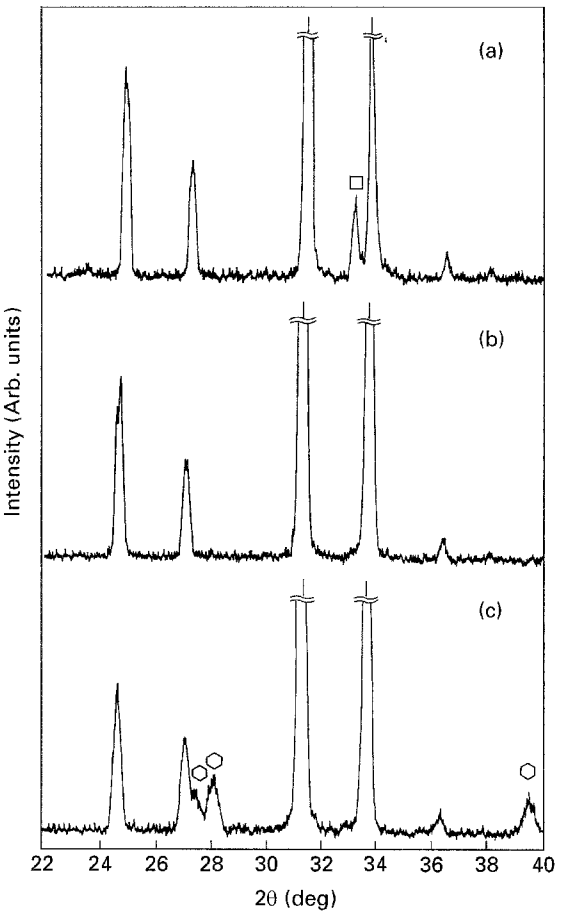

Figure 3 Magnified XRD patterns of ternary oxides sintered and annealed as in Fig. 2. (a) Sample F (La:Sr:Cu = 1.75:0.15:1), (b) sample G (La:Sr:Cu = 1.80:0.15:1), and (c) sample H (La:Sr:Cu = 1.95:0.15:1). (□) $La_{1.67}Sr_{0.33}Cu_2O_{5-\delta}$, (○) $La(OH)_3$.

Note that in lanthanum-deficient samples, crystalline CuO was not detected.

Sample H, with excess lanthanum (La:Sr:Cu = 1.95:0.15:1), only shows the presence of $La(OH)_3$ (Fig. 3c).

Sample I (La:Sr:Cu = 1.67:0.33:2) shows the non-superconducting phase $La_{1.67}Sr_{0.33}Cu_2O_{5-\delta}$ contaminated with impurities revealed by the reflections appearing at 2θ = 24.6°, 27.0°, 31.2°, 32.4°, 33.6°, 43.6° and 48.2° (Fig. 4a). These signals might be assigned to either La_2CuO_4 or $La_{1.85}Sr_{0.15}CuO_4$ and possibly to the non-oxygen-deficient perovskite $LaCuO_3$ (PDF 25–291). Note that these spurious phases persist in the solid even after the thermal treatments performed to obtain the sintered pellets (Fig. 4b).

Table II summarizes the main features observed in the diffractograms of the sintered pellets.

3.2. Iodometric titration

The *y* values shown in Table III were calculated using the equation proposed by Appelman *et al.* [4]. The atomic ratios used for these calculations were La:Cu = 2.00:1 for samples A–E, La:Sr:Cu = 1.85:0.15:1 for samples F–H and La:Sr:Cu = 1.67:0.33:2 for sample I.

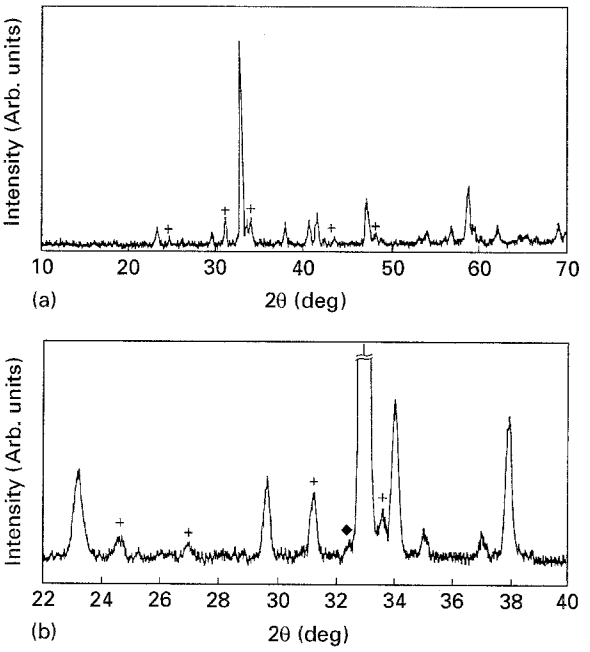

Figure 4 XRD patterns of sample I (La:Sr:Cu = 1.67:0.33:2). (a) Calcined powder as in Fig. 1 (2θ = 10°–70°), and (b) after sintering and annealing as in Fig. 2 (2θ = 22°–40°). (+) La_2CuO_4–$La_{1.85}Sr_{0.15}CuO_4$, (◆) $LaCuO_3$.

TABLE II Composition and crystalline phases of binary and ternary oxides[a]

La:(Sr):Cu ratio	Impurity phases
2.00:1	None
1.95:1	None
1.90:1	None
1.85:1	Trace CuO
1.70:1	Slight CuO
1.75:0.15:1	$La_{1.60}Sr_{0.40}Cu_2O_{5-\delta}$
1.80:0.15:1	None
1.95:0.15:1	La_2O_3, $La(OH)_3$
1.67:0.33:1	$La_2CuO_4La_{1.85}Sr_{0.15}CuO_4/LaCuO_3$
1.85:0.15:1 [2]	None

[a] After sintering and annealing in flowing oxygen.

TABLE III Oxygen content of La–Cu–O and La–Sr–Cu–O powders obtained by iodometric analysis

Sample	Mass (mg)	$\bar{y}$[a]	S.D.	$\bar{y} \pm 3$S.D.
A	85.00	4.0072	0.000 10	4.0072 ± 0.0003
B	85.00	4.0076	0.000 64	4.0076 ± 0.0014
C	85.00	4.0068	0.000 69	4.0068 ± 0.0021
D	85.00	4.0068	0.000 69	4.0068 ± 0.0021
E	85.00	4.0079	0.000 64	4.0079 ± 0.0019
F	80.00	4.0017	0.000 75	4.0017 ± 0.0023
G	80.00	4.0008		
H	80.00	3.9925	0.000 69	3.9925 ± 0.0021
I	46.80	4.9924		
From [3][b]	85.00	3.9987		

[a] Mean value, $n = 3$.
[b] La:Sr:Cu = 1.85:0.15:1.

3.3. SEM observations

Fig. 5a shows an overall view of sample A fragments (La:Cu = 2:00:1) as obtained following the thermal treatment. It shows globular formations with pores of varying size which defines a surface with irregular profile. Fig. 5b and c shows at higher magnification a compact microstructure made up of polyhedric grains of well-defined borders smaller than 5 μm. In this solid, most grains revealed the presence of lamellae sets with a typical thickness of the order of 0.1 μm. Less frequently, particles of roughly 0.2–0.3 μm were observed as inclusions of intergranular and intragranular regions (Fig. 5d).

3.4. Temperature-programmed reduction

Figs 6 and 7 show the reduction profiles of samples A–I. Sample A (La:Cu = 2.00:1) shows the maximum hydrogen consumption at 730 K accompanied by a lower intensity peak centred at 606 K (Fig. 6a). Similar behaviour was observed in the lanthanum-deficient samples B–E. With increasing lanthanum deficiency, the lower temperature peak (611–619 K) becomes better defined while the resolution of the other peaks is also affected. On the other hand, the maximum hydrogen consumption peak temperature does not correlate with lanthanum deficiency. The reduction of all these samples starts at around 540 K and ends at 800 K (Fig. 6b–e).

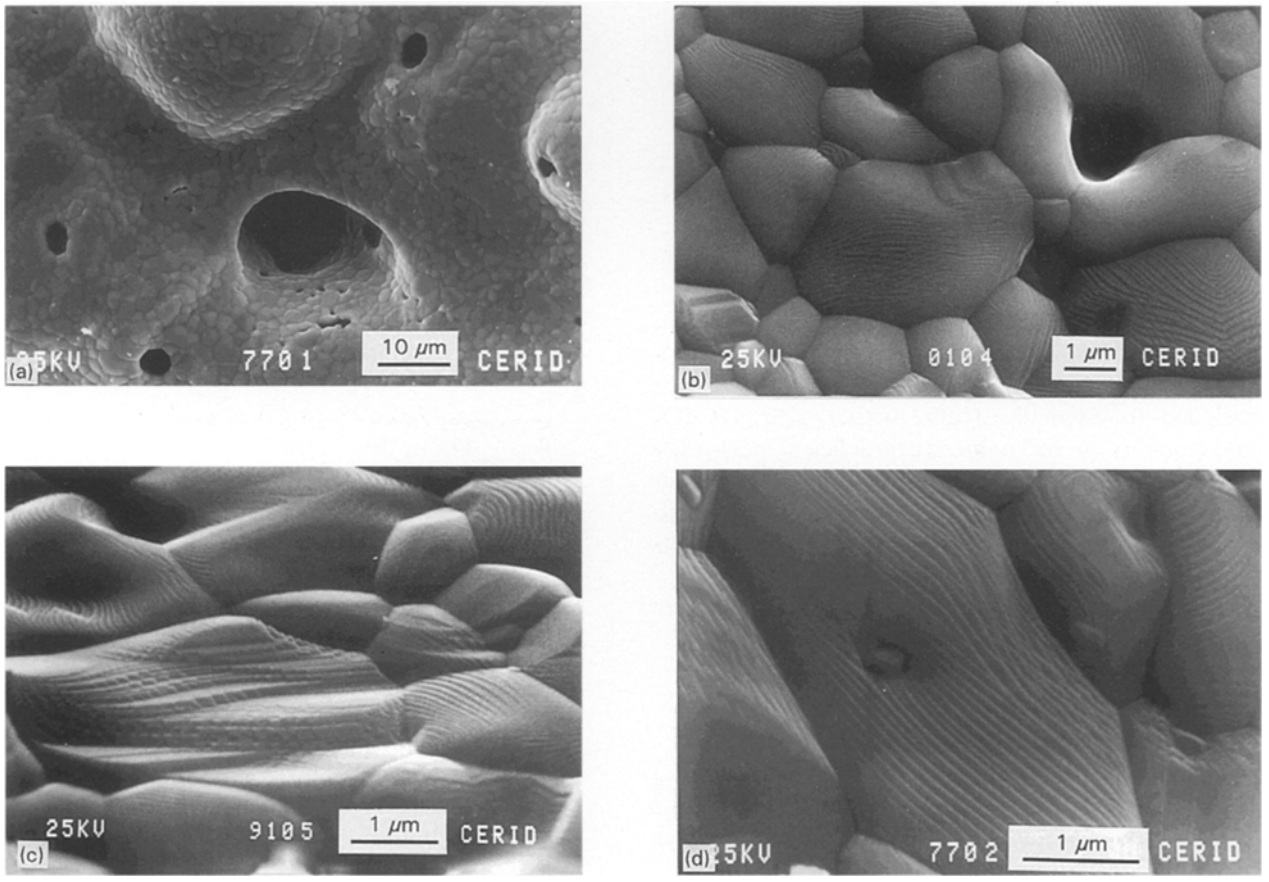

Figure 5 Morphological features of sample A (La:Cu = 2.00:1) before grinding. (a) Irregular surface, (b) packing of polyhedral grains, and (c, d) growth layers or hillock.

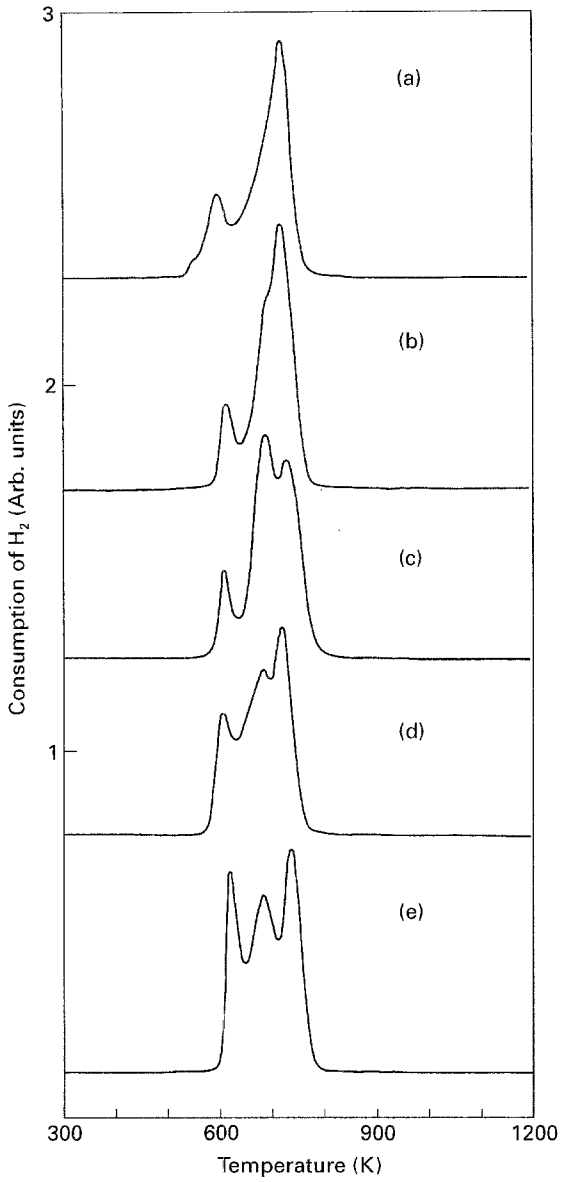

Figure 6 TPR profiles of binary oxides calcined as in Fig. 1. (a) Sample A (La:Cu = 2.00:1), (b) sample B (La:Cu = 1.95:1), (c) sample C (La:Cu = 1.90:1), (d) sample D (La:Cu = 1.85:1), and (e) sample E (La:Cu = 1.70:1).

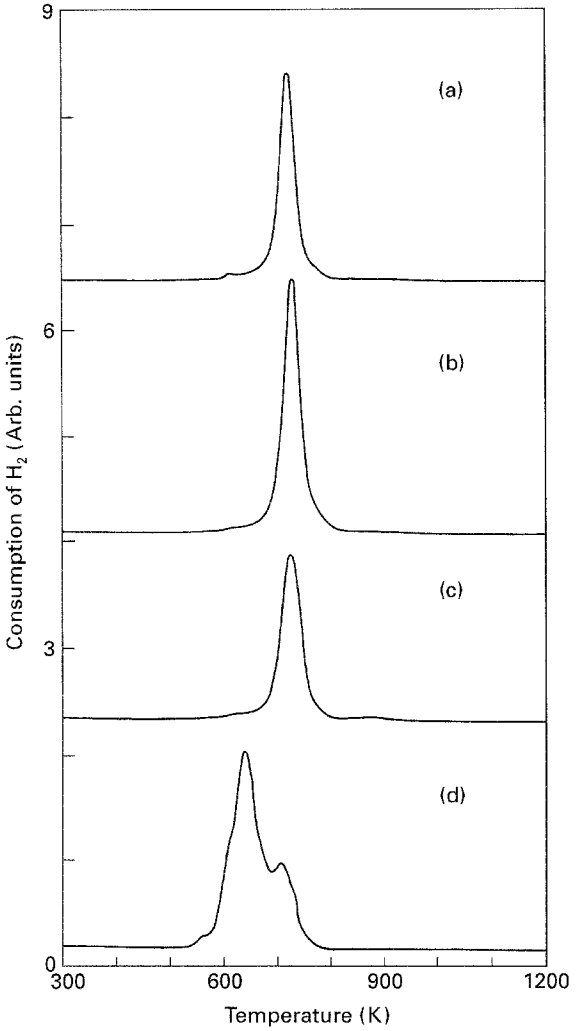

Figure 7 TPR profiles of ternary oxides as in Fig. 1 (a) Sample F (La:Sr:Cu = 1.75:0.15:1), (b) sample G (La:Sr:Cu = 1.80:0.15:1), (c) sample H La:Sr:Cu = 1.95:0.15:1), and (d) sample I (La:Sr:Cu = 1.67:0.33:2).

In the ternary oxides F, G and H with La:Sr:Cu = 1.75:0.15:1, 1:80:0.15:1 and 1:95:0.15:1, the reduction occurs in a single step centred around 725–730 K. The profiles show that reduction starts at ~ 580 K and ends at 800 K (Fig. 7a–c).

Several peaks appeared in sample I (La:Sr:Cu = 1.67:0.33:2), indicating that the reduction occurs in several steps in the temperature range 534–800 K (Fig. 7d). The maximum hydrogen consumption is now centred at 640 K.

4. Discussion

4.1. Composition and crystalline phases

4.1.1. La–Cu–O system

The X-ray data show that it is not possible to obtain a monophasic powder when the freeze-dried precursor with La:Cu = 2.00:1 is calcined at 1253 K for 8 h. The impurities detected (CuO and $La(OH)_3$) indicate incomplete conversion to La_2CuO_4 which is completed after sintering and annealing in oxygen (Figs 1 and 2a).

Similarly to what has been reported for $La_{1.85}Sr_{0.15}Cu_4$ [2], the partial melting of the precursors at around 600 K becomes the limiting factor which precludes the synthesis of La_2CuO_4 at lower temperatures.

The lanthanum-deficient samples B–E also contain similar impurities. Minimum amounts were detected in sample C (La:Cu = 1.90:1) containing traces of $La_2O_2CO_3$ and possibly CuO. This is probably due to incomplete reaction (caused by heterogeneity in the starting materials) for it is possible to reach total conversion after sintering and annealing in oxygen.

In view of this, CuO should be detected as impurity in samples B–E. In fact, the X-ray patterns confirmed the presence of CuO in sintered pellets of compositions La:Cu $\leq$ 1.85:1 (Fig. 2c). Therefore, it may be possible to obtain monophasic oxides in the composition range La:Cu = 2.00–1.90:1 (Fig. 2a and b). Note, however, that the amount of excess CuO which should be present in samples B and C (Table I), if their compositions do not differ from the nominal values, is 0.5 and 1.0 wt/wt%, respectively. Thus, the absence of CuO in the diffractograms may be due to lack of

sensitivity rather than a variation in the lanthanum stoichiometry.

Several authors [7–9] have reported that the most favourable La:Cu ratio to obtain La_2CuO_4 is slightly lower than 2. In this vein, Lewandowski *et al.* [10] have reported that the K_2NiF_4-type phase in the La–Co–O system is lanthanum deficient with one-twelfth of the lanthanum sites vacant, yielding a La/Co ratio of 1.83 rather than 2.00. They proposed a new stoichiometry for these compounds represented by $La_{1.85}CoO_{4-\delta}$ with $0 \leq \delta \leq 0.15$. However, for La_2CuO_4 with the same structure, it is generally agreed that no lanthanum vacancies are present [11–13].

4.1.2. La–Sr–Cu–O system

The diffractograms of samples F and G show that the thermal decomposition of lanthanum-deficient precursors leads to powders containing the following crystalline phases: $La_{1.85}Sr_{0.15}CuO_4$, La_2O_3/$La(OH)_3$ and $La_{1.67}Sr_{0.33}Cu_2O_{5-\delta}$. This behaviour has also been observed in stoichiometric precursors La:Sr:Cu = 1.85:0.15:1 [2]. After sintering and annealing in oxygen, monophasic pellets were obtained due to the occurrence of the following reaction [2]

$$La_{2-z}Sr_zCu_2O_5 + [2(1+p)]\ La(OH)_3 + p\ CuO \rightarrow (2+p)\ La_{2-y}Sr_yCuO_4 + [3(1+p)]H_2O \quad (1)$$

where $p = 2 - y$. The structural evolution observed in samples F and G after sintering and annealing in oxygen is consistent with this mechanism. A limited lanthanum deficiency (La:Sr:Cu = 1.80:0.15:1) still allows the synthesis of a monophasic oxide. However, if this deficiency increases (La:Sr:Cu = 1.75:0.15:1), the superconducting phase coexists with $La_{1.67}Sr_{0.33}Cu_2O_{5-\delta}$ as impurity (Fig. 3a and b). This result is consistent with the phase diagram of the La_2O_3–SrO–CuO system [14]. The phase diagram also shows at these compositions the presence of CuO which was not detected by XRD in any of the solids prepared.

The synthesis of a monophasic solid with La:Sr:Cu = 1.80:0.15:1 brings up again the possible existence of lanthanum vacancies. Chiang *et al.* [15] have proposed that the composition of the equilibrated monophasic compound may be represented by the following stoichiometry: $La_{1.85-x}Sr_{0.15}CuO_4$. Furthermore, Braden *et al.* [16] have reported the detection of roughly 1% vacancies in the site occupied by La/Sr. They studied the neutron diffraction patterns of single crystals of $La_{2-x}Sr_xCuO_{4\pm\delta}$.

In the case of excess lanthanum, the phase diagram shows the coexistence of $La_{1.85}Sr_{0.15}CuO_4$ and La_2O_3 as was the case for sample H, La:Sr:Cu = 1.95:0.15:1 (Fig. 2c). La_2O_3 is easily hydrated and this is why the sintered pellets usually disintegrate as reported previously [5]. Note that despite the compositional heterogeneity induced by partial melting of the precursors, the formation of the non-superconducting oxide is inhibited by excess La_2O_3.

The presence of impurities in sample I (La:Sr:Cu = 1.67:0.33:2) even after sintering and oxygen annealing may be explained if it is accepted that the composition of the non-superconducting phase differs somewhat from the above stoichiometry. In fact, Huang *et al.* [17] observed the presence of similar phases in the sintered solid obtained from La_2O_3, CuO and $SrCO_3$ in the proportion needed to synthetize $La_{1.67}Sr_{0.33}Cu_2O_{5-\delta}$.

On the other hand, the formation of the superconducting phase and CuO is expected from the phase diagrams [14] when trying to synthesize the compound $La_{8-x}Sr_xCu_8O_{20-\delta}$ for $x < 1.6$. Our results thus confirm those of De Leeuw *et al.* [14] and Murayama *et al.* [18] who reported the formation of a solid solution for $1.6 \leq x \leq 2.0$. These results are at variance with those of Er-Rakho *et al.* [19] and Tokura *et al.* [20] who reported the production of monophasic compounds with lower strontium content.

In view of the above, it is likely that the non-superconducting phase which appears when trying to obtain $La_{1.85}Sr_{0.15}CuO_4$ from either stoichiometric or lanthanum-deficient precursors, is not $La_{1.67}Sr_{0.33}Cu_2O_{5-\delta}$. Instead, its composition should be represented by La:Sr:Cu = 1.60:0.40:2 in disagreement with Payzant *et al.* [21]. However, the different stoichiometry should not affect the reaction scheme suggested [21] for the formation of this impurity phase.

4.2. Oxygen stoichiometry

The y values for the binary samples A–E do not show any statistically significant differences. This y value coincides with data reported in the literature for La_2CuO_4 [4]. The impurities detected in the diffractograms are not enough to modify the calculated y value.

The ternary oxides obtained from lanthanum-deficient precursors (samples F and G show slight excess of oxygen compared to monophasic powder of nominal composition (Table III). This difference may be due to the presence of the non-superconducting phase as residual impurity.

Note, however, that sample G becomes monophasic after sintering and annealing in oxygen (Fig. 3b). To interpret these data, the crystallographic model of Galy *et al.* [22] may be applied for oxygen understoichiometry of basic M_2CuO_4 structure (K_2NiF_4-type) with $M_2 = La_{2-x}Sr_x$. They suggest that in order to reach $y < 4$ it is necessary to eliminate a layer of $(MO)_n$ parallel to the $[\bar{1}01]$ plane. Following this deformation, the structure may collapse to form a lattice with the general formula $M_{2-\delta}CuO_{4-\delta}$. This means that oxygen sub-stoichiometry must be accompanied by non-stoichiometry of M. The chemistry related to their system should be represented as $La_{2-x}Sr_{x-\delta}Cu^{2+}_{1-x}Cu^{3+}_xO_{4-\delta}$ or $La_{2-\delta}CuO_{4-\delta}$.

The oxygen content calculated from the experimental Cu(III) fraction considering the ratio La:Sr:Cu = 1.80:0.15:1 is $y = 3.9242$ ($\delta = 0.0758$). The same calculations performed for the lanthanum-deficient samples B and C yield $y = 3.9324$

($\delta = 0.0676$) and $y = 3.8565$ ($\delta = 0.1435$), respectively. These δ values are consistent with the model proposed by Galy *et al.* [22] which allows an explanation for the small variations in composition detected in these mixed valence copper oxides.

Because the uncertainty in determining y is ± 0.0021, the oxygen content of sample H (La:Sr:Cu = 1.95:0.15:1) is lower than the values determined in monophasic powders of nominal composition (Table III). This deficiency might be due to the error involved in considering that 100% of the sample is $La_{1.85}Sr_{0.15}CuO_4$, while the corresponding diffractogram shows that it contains a measurable amount of $La(OH)_3$.

If the y value for sample I is calculated on the basis of the stoichiometric ratio La:Sr:Cu = 1.60:0.40:2, $y = 4.9561$ results. The oxygen deficiency now becomes coincident with the value reported by Er-Rakho *et al.* [19] for the oxide $La_{6.4}Sr_{1.6}Cu_8O_{19.84}$. Note that the impurities present which are included in the experimental value do not affect the absolute value of y.

4.3. Surface morphology

The macrostructure observed in Fig. 5a (sample A, La:Cu = 2.00:1) is characteristic of partial melting of the precursor during thermal treatment. The globular formations and macropores originate in the sudden expulsion of gases through a viscous quasi-liquid phase. The same picture was observed in the ternary oxides [2]. In both cases the selection of high heating rates (50 K min^{-1}) coupled with $T_f = 1253$ K and slow cooling rates (1 K min^{-1}) leads to a microstructure made up of grains in the 3–5 μm range ([2], Fig. 5b) which reflect the sintering of melted oxides.

The pyramid (or hillock) structures observed in almost all grains (Fig. 5c and d) are similar to those described by Sun *et al.* [23] in single crystals of YBCO grown using the CuO-flux technique. These structures result from the interaction of many screw dislocations according to the growth mechanism advanced by these authors. The square spiral morphology of some grains (Fig. 5d) was associated with low temperature of formation and indicates that the growth anisotropy of the different crystallographic direction became pronounced.

The differences detected in the morphology in the growth spirals in samples of composition La:Sr:Cu = 1.85:0.15:1 (circular) [2] and La:Cu = 2.00:1 (square) may be related to differences in the height of the spiral gauge. Sun *et al.* [23] have reported that the smaller this dimension, the lower was the polygonalization of the spiral observed.

On the other hand, Marella *et al.* [24] have observed that the presence of rectangles in platelets grown from partially melted bulk $YBa_2Cu_3O_{7-\delta}$ may be explained by the presence of a fine dispersion of particles of secondary phases such as $Y_2Ba_2CuO_5$ or CuO. The details illustrated in Fig. 5d would indicate that both effects could explain the surface morphology of La_2CuO_4 and $La_{1.85}Sr_{0.15}CuO_4$.

4.4. Reduction of cuprates

The TPR profiles of samples A–E (La:Cu = 2.00–1.70:1) are characterized by the presence of three reduction peaks (Fig. 6). The 606–619 K signal may be assigned to CuO reduction (detected by XRD). The reduction peak of pure CuO calcined at 1213 K (5 h) occurs at 611–640 K [15]. This assignment is also consistent with the increasing size of this signal with decreasing La/Cu ratios. The other two higher temperature peaks are assigned to the reduction of La_2CuO_4. The results seem to indicate that Cu^{2+} reduces to Cu^0 in two steps, involving Cu^+, as proposed by Ueda *et al.* [25].

The reduction profiles of the ternary samples F, G and H show a single reduction peak except for a low-intensity signal observed for sample F at 613 K (Fig. 7a–c). Note that varying the lanthanum composition does not affect either the profiles or the reducibility of these solids. The maximum hydrogen consumption observed at 725–730 K is very close to the values reported for monophasic powders La:Sr:Cu = 1.85:0.15:1 [3]. These results are not coincident with those reported by Ueda *et al.* [25] for $La_{2-x}Sr_xCuO_4$ ($x = 0, 0.15, 0.3$ and 0.6). These authors have suggested that the partial substitution of Sr^{2+} for La^{3+} accelerates the reduction of copper. They also reported a significant decrease in the intensity of the peak assigned to Cu^+ reduction with increasing Sr^{2+} content. In fact, the sample with $x = 0.6$ showed a single reduction peak.

The TPR profile assigned to sample I (La:Sr:Cu = 1.67:0.33:2) reflects a more complex behaviour characterized by the presence of several reduction peaks (Fig. 7d). The maximum hydrogen consumption at 640 K indicates that this sample is easier to reduce than La_2CuO_4 (Fig. 6a) and $La_{1.85}Sr_{0.15}CuO_4$ [3] but similar to CuO [26].

The reduction process occurring in several steps may be ascribed to the type of oxygen-deficient perovskite structure affected by the presence of impurities.

5. Conclusions

The synthesis of La_2CuO_4 by thermal decomposition of freeze-dried precursors at a final temperature of 1253 K (8 h) does not lead to a monophasic solid. The total conversion to the desired product is achieved after sintering (1253 K, 12 h) and annealing in oxygen (773 K, 6 h). The limiting factor in this process is the formation of a transient liquid phase at around 600 K which has already been observed in ternary mixtures of acetates [2].

The study of lanthanum-deficient formulations allowed the detection of small variations in the stoichiometry of solids $La_{2-x}Sr_xCuO_4$ with $x = 0$ and 0.15. Monophasic sintered pellets were obtained with the following starting compositions: La:Cu = 1.95:1 and 1.90:1 and La:Sr:Cu = 1.80:0.15:1. Lower lanthanum contents lead to the appearance of CuO in solids with $x = 0$ or the non-superconducting phase $La_{1.60}Sr_{0.40}Cu_2O_{5-\delta}$ in samples with $x = 0.15$. The experimental evidence presented here is consistent with a crystallographic model proposed by Galy *et al.*

[22] which describes the formation of phases $M_{2-\delta}CuO_{4-\delta}$, where $M_2 = La_{2-x}Sr_x$.

The structural evolution observed in samples with $x = 0.15$ confirmed the effect of lanthanum composition in the formation of the ternary non-superconducting oxide and its reaction according to the scheme proposed previously for $La_{1.85}Sr_{0.15}CuO_4$ [2]. Indeed, the synthesis of the non-superconducting phase from freeze-dried precursors of composition La:Sr:Cu = 1.67:0.33:2 indicated that its stoichiometry is better represented by $La_{1.60}Sr_{0.40}Cu_2O_{5-\delta}$, a result which is consistent with the phase diagram of the La_2O_3–SrO–CuO system.

A detailed observation of the partially melted oxides of composition La:Cu = 2:00:1 allowed the identification of growth arcs and spirals of square-shaped morphology. These observations suggest a screw dislocation growth mechanism along the *c*-axis similar to that observed in epitaxially grown thin films and single crystals, obtained using the flux method [23].

The reduction of the cuprates occurs between 550 and 800 K. The different TPR profiles can be associated with the formation of more or less stable intermediates which could be identified through *in situ* experiments at high temperature using techniques such as XRD and EPR.

Acknowledgements

This work was supported by a grant from CONICET PID 3-0956/88. The authors also thank Professor N. Pratta for her assistance with the scanning electron microscopy, Professor E. Grimaldi for her assistance with the English version, and the Department of Biological Chemistry for making the freeze-drying apparatus available.

References

1. S. ALCONCHEL, M. ULLA and E. LOMBARDO, *Mater. Sci. Eng. B.*, submitted.
2. *Idem, J. Mater. Sci.*, in press.
3. *Idem, Mater. Sci. Eng. B.*, **27** (1994) 117.
4. E. APPELMAN, L. MORSS, A. KINI, V. GEISER, A. UMEZAWA, G. CRABTREE and K. CARLSON, *Inorg. Chem.* **26** (1987) 3237.
5. S. ALCONCHEL, PhD thesis, Universidad Nacional del Litoral, Santa Fe, Argentina (1993).
6. Powder Diffraction File, JCPDS, International Center for Diffraction Data, Swarthmore, PA (1991).
7. S. FINE, M. GREENBLATT, S. SIMIZU and S. FRIEDBERG, *Phys. Rev. B* **36** (1987) 5716.
8. S. SHAHEEN, N. JISRAMI, Y. LEE, Y. ZHANG, M. CROFT, W. McLEAN, H. ZHEN, L. REBELSKY and S. HORN, *ibid.* **36** (1987) 7214.
9. N. KIEDA, S. NISHIYAMA, K. SHINOZAKI and N. MIZUTANI, *Solid State Ionics* **49** (1991) 85.
10. J. LEWANDOWSKI, R. BEYERLEIN, J. LONGO and R. McCAULEY, *J. Am. Ceram. Soc.* **69** (1986) 699.
11. B. DABROWSKY, D. HINKS, J. JORGENSEN, K. ZHANG and C. SEGRE, *Bull. Am. Phys. Soc.* **33** (1988) 557.
12. J. SCHIRBER, B. MOROSIN, R. MERILL, P. HLAVA, E. VENTURINI, J. KWAK, P. NIGREY, R. BAUGHMAN and D. GINLEY, *Phys. C* **152** (1988) 121.
13. J. JORGENSEN, B. DABROWSKI, S. PEI, D. HINKS, L. SODERHOLM, B. MOROSIN, J. SCHIRBER, E. VENTURINI and D. GINLEY, *Phys. Rev. B* **38** (1988) 11337.
14. D. DE LEEUW, H. MUTSAERS, G. GEELEN and C. LANGEREIS, *J. Solid State Chem.* **80** (1989) 276.
15. Y. CHANG, D. RUDMAN, D. LEUNG, J. IKEDA, A. ROSHKO and B. FABES, *Phys. C* **152** (1988) 77.
16. M. BRADEN, G. HEGER, P. SCHWEISS, Z. FISK, K. GAMAYUNOV, I. TANAKA and H. KOJIMA, *ibid.* **191** (1992) 455.
17. T. HUANG, A. NAZZAL, Y. TOKURA, J. TORRANCE and R. KARIMI, *Powder Diffract.* **3** (1988) 81.
18. N. MURAYAMA, S. SAKAGUCHI, F. WAKAI, E. SUDO, A. TSUZUKI and Y. TORÜ, *J. Appl. Phys. Jpn* **27** (1988) L55.
19. L. ErRAKHO, C. MICHEL and B. RAVEAU, *J. Solid State Chem.* **73** (1988) 514.
20. Y. TOKURA, J. TORRANCE, A. NAZZAL, T. HUANG and C. ORTTIZ, *J. Am. Ceram. Soc.* **109** (1987) 7555.
21. E. PAYZANT, H. KING and J. WALLACE, *Solid State Commun.* **76** (1990) 409.
22. J. GALY, M. CASANOVE, A. ALIMOUSSA and C. ROUCAU, private communication (1993).
23. B. SUN, K. TAYLOR, B. HUNTER, D. MATTHEWS, S. ASHBY and K. SEALY, *J. Crystal Growth* **108** (1991) 473.
24. M. MARELLA, G. DINELLI, B. BURTET FABRIS and B. MOLINAS, *J. Alloys Compounds* **189** (1992) 123.
25. A. UEDA, Y. OKAMOTO and T. IMANAKA, *Chem. Express* **3** (1988) 723.
26. I. HALASZ, H. JEN, M. SHELEF, S. KAO and K. SIMON, *J. Solid State Chem.* **92** (1991) 327.

Received 20 May
and accepted 4 October 1994